CHAPTER THREE

GLOBAL CLIMATE CHANGE SCIENCE

FLOODED ROAD, WESTERN AUSTRALIA, ISTOCK

CHAPTER 3 GLOBAL CLIMATE CHANGE SCIENCE

This chapter introduces the global climate system, how it varies naturally, and the concept of external forcing of the climate system, global trends and their causes. It also introduces global climate models and the external forcing scenarios that are used to run climate model experiments that are the basis for many of the results presented in this Report.

3.1 FACTORS DRIVING CLIMATE VARIABILITY AND CHANGE

Climate variability occurs naturally within the climate system, due to the 'internal' interaction of physical processes, for example through chaotic processes or through exchanges of heat within, and between the atmosphere and ocean.

A second source of influences on the climate arises from changes in factors 'external' to the climate system. Examples of these are changes to atmospheric composition from volcanic activity or anthropogenic (human) activities, or changes in output of the Sun (solar radiation) or changes in the Earth's orbit around the Sun. What these have in common is that they alter the balance of radiation of the Earth/atmosphere system, by changing the absorbed or reflected solar radiation or by changing the absorption characteristics of the radiation emitted by the Earth. In simple terms, the Earth must then respond by further changing these fluxes to restore radiative balance.

The effects of 'naturally occurring' external factors (principally the solar cycle and volcanic activity) can be considered part of the natural climate variability.

'Climate change' refers to long-term (typically decades or longer) changes in the properties of the climate, such as the mean or variability. Climate change can arise from both internal processes and from external factors, natural and anthropogenic.

'Anthropogenic climate change', in particular, is that which originates from the Earth's response to the long-term 'external' radiative imbalance caused by human activities.

The measure of the imbalance imposed by external factors is termed 'radiative forcing', as it 'forces' an adjustment to the Earth's natural balance of incoming and outgoing radiation. Radiative forcing (sometimes called 'climate forcing') is the net measure of incoming and outgoing radiation and is measured at the tropopause or top of the atmosphere. A negative forcing acts to cool the climate system, whereas positive forcing has a warming impact.

3.1.1 INTERNAL ("UNFORCED") CLIMATE VARIABILITY

Natural oscillations and variations occur within the climate system across the full range of spatial and temporal timescales. Variations occur from daily synoptic timescales, involving the passage of high and low pressure systems ('weather'), through to seasonal variations such as monsoon systems and interannual variations due to processes such as El Niño Southern Oscillation (ENSO) and the Indian Ocean Dipole (IOD) (see Chapter 4), and to decadal variability from processes such as the Interdecadal Pacific Oscillation (IPO).

Typically, climate variability involves the exchange of heat, moisture and momentum between or within the atmosphere, ocean and land surface, marked by transient changes to the total heat within the climate system. By contrast, climate change is characterised by changes to the long-term storage or redistribution of heat. The vast heat capacity of the ocean acts as both the 'buffer' associated with very long (*e.g.* decadal) timescale climate variability and as the long-term accumulator of heat under climate change (Church *et al.* 2005).

Although climate variability occurs on all scales, its magnitude becomes larger as spatial scales decrease. For example regional rainfall variability is greater than continental scale variability, which is greater in turn than that at global scales. Furthermore, variability has different characteristics for different features. For example rainfall is highly spatially and temporally variable, relative to mean values. It will be seen below that these features of variability have important implications for the detection and attribution of climate change, as climate variability can often 'mask' climate change, particularly at regional or local scales (see Chapter 4). Long- and short-term variability can additionally oppose or reinforce future climate changes (refer Chapter 6) and must be factored into the 'envelope' of projected changes.

3.1.2 EXTERNAL FORCING FACTORS

Estimates of anthropogenic and natural external forcing are presented in Figure 3.1.1. For each gas, the forcing is shown as a function of its emissions rather than its final atmospheric concentrations.

Greenhouse gases produce positive forcing from increased trapping of outgoing longwave radiation, along with some additional absorption of solar radiation. Water vapour is an important greenhouse gas, however, its residence time in the atmosphere is short, and water vapour amounts are not directly affected by humans. Rather, water vapour concentrations respond to temperature increases arising from initial forcing by the long lived greenhouse gases, thereby further reinforcing (amplifying) the warming that occurs.

The best estimate of the forcing from changes in the long-lived greenhouse gases (carbon dioxide, methane, nitrous oxide and halocarbons) is around 3.0 W/m^2 (watts per square metre) (Figure 3.1.1). Carbon dioxide is the largest contributor, at around 1.7 W/m^2. Isotopic evidence, carbon dioxide concentration distributions and a measured decrease in atmospheric oxygen together provide overwhelming evidence that human activities have been responsible for these changes in greenhouse gas concentrations (IPCC, 2013).

These gases are 'long-lived' in the atmosphere, and as a consequence their geographical concentrations are relatively homogeneous (*i.e.* evenly spread). Carbon dioxide lifetime in the atmosphere is hard to quantify simply, because it is a result of many different cycles and processes, with a wide range of timescales. Around half the emitted carbon dioxide is currently being absorbed by the ocean and terrestrial biosphere (IPCC, 2013, Chapter 6), with the remainder contributing to increased atmospheric CO_2 concentrations. The 'adjustment time' (*i.e.* the time taken to permanently remove the increased CO_2 concentration from the atmosphere) is of the order of centuries.

Land use changes have produced a small net negative forcing globally, mainly due to the clearing of (low reflectivity) forests, and their replacement by (higher reflectivity) crop or pastureland, and the difference in snow characteristics over cleared versus forested terrain (IPCC, 2013). Land use changes can also potentially have impacts on regional temperatures and rainfall, such as in south-west Western Australia (Pitman *et al.*, 2004, Timbal and Arblaster, 2006). Land-use change also impacts on the carbon budget, and globally have significantly increased carbon levels in the atmosphere (IPCC, 2013).

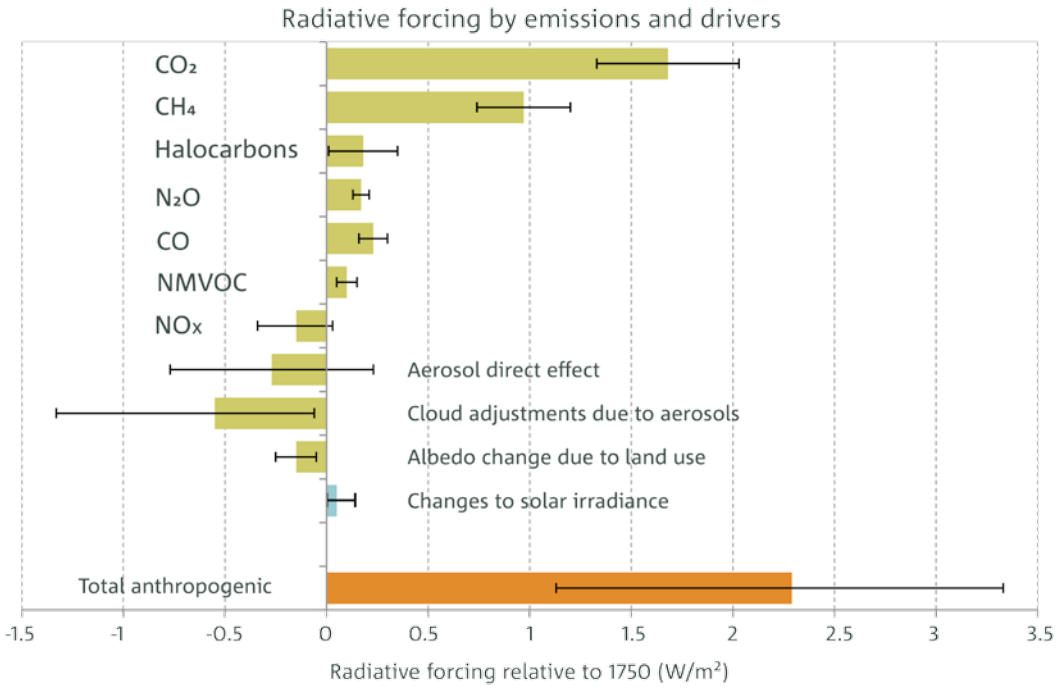

FIGURE 3.1: RADIATIVE FORCING ESTIMATES IN 2011 WITH RESPECT TO PRE-INDUSTRIAL CONDITIONS (1750) FROM EMISSIONS AND DRIVERS. FOR EACH GAS, THE FORCING IS SHOWN AS A FUNCTION OF ITS EMISSIONS RATHER THAN ITS FINAL CONCENTRATIONS. FOR EXAMPLE THE IMPACT OF EMITTED HALOCARBONS ON REDUCING STRATOSPHERIC OZONE CONCENTRATIONS AND CONSEQUENT RADIATIVE FORCING IS INCLUDED UNDER HALOCARBONS, GREEN BARS SHOW ANTHROPOGENIC EMISSIONS AND DRIVERS, BLUE ARE NATURAL, AND THE ORANGE BAR SHOWS THE TOTAL ANTHROPOGENIC FORCING. BARS REPRESENT THE 90 % CONFIDENCE RANGE. NMVOC REPRESENTS NON-METHANE VOLATILE ORGANIC COMPOUNDS SUCH AS BENZENE AND ETHANOL (ADAPTED FROM: FIGURE SPM.5 IN IPCC, 2013).

Solar cycles or changes in the orbit of the Earth can affect the amount of incoming solar radiation. Variability of the sun is imperfectly understood, but the well-established 11 year sunspot cycle alters total solar output by around 0.08 % (IPCC 2013, Chapter 8), which has only minor impact on climate (Meehl *et al*. 2009). The best estimate for net solar output change from 1750 to present, derived from several proxies, is for a forcing of 0.05 W/m^2 (Figure 3.1.1). Direct measurements from space over the last 30 years suggest a small reduction in forcing for this period of -0.04 W/m^2. Forcing from solar changes is dwarfed by those from anthropogenic sources, indicating the Sun has played little role in observed changes (Section 3.4).

Ozone in the stratosphere results from ultraviolet interaction with oxygen. In the troposphere it results from chemical transformation of other gases such as carbon monoxide or nitrous oxide. Ozone concentration changes have a varying impact depending on their location within the atmosphere. Increases in the lower atmosphere (troposphere) have caused a warming, due to their trapping of outgoing radiation. Stratospheric decreases in ozone (due to destruction by chlorofluorocarbons (CFCs), and related to the 'ozone hole') have resulted in a negative forcing from decreased absorption of outgoing radiation. Forcing for ozone is not shown explicitly in Figure 3.1.1, but is included under its precursor emissions (CFCs, carbon monoxide, nitrous oxide).

Aerosols are tiny solid or liquid particles suspended in the atmosphere. They have a 'direct' impact on radiation by reflecting incoming solar radiation back to space. They additionally have an 'indirect' impact on radiation by affecting the distribution, lifetime and type of clouds through their role as cloud condensation nuclei (*i.e.* particles on which water vapour can condense, as part of the process in forming water droplets). Forcing from aerosol changes is highly uncertain, with the best estimate of around -0.9 W/m^2 (IPCC, 2013). Aerosol characteristics differ dramatically from greenhouse gases, in that their lifetimes in the atmosphere are short (of the order days to weeks) and their distribution is not uniform within the atmosphere, with large concentrations downwind of industrial areas. There are additionally large natural sources of aerosols, including dust from arid inland regions of Australia (Mitchell *et al*. 2013) and sea salt particles arising from the oceans (any trends in these are not explicitly included in Figure 3.1.1)

Volcanic eruptions can deposit large amounts of dust and sulphate aerosols into the atmosphere, increasing the reflection of incoming solar radiation, producing a negative (cooling) forcing. Most volcanoes have only minor radiative impact, but large explosive volcanoes can inject aerosols directly into the stratosphere, where they can persist for months or years causing significant forcing. It is estimated that Mount Pinatubo induced a short-term cooling of around 0.5 °C, peaking a year or so after eruption (Soden *et al*. 2002). The carbon dioxide emitted by volcanoes, however, is negligibly small compared to anthropogenic emissions (Morner and Etiope, 2002). Volcanoes are not included in Figure 3.1.1, as they provide only transient forcing, and there is no evidence that volcanic activity has changed since pre-industrial times.

Urban heat island effects describe the warming influence on urban regions from their built environment. They operate in all seasons, and are usually greater at night (Trewin, 2010). They are included in Figure 3.1.1 under land use changes but their global impact is relatively small. They may however, have significant local impacts, and must be considered for urban projections. Stations that have experienced the urban heat island effect have been removed from the temperature record for detection and attribution purposes (see Section 4.2).

Net forcing describes the best estimate of anthropogenic global net forcing and is assessed to be around 2.3 W/m^2 since 1750. This value dwarfs natural external forcing (Figure 3.1.1).

3.2 EMISSIONS SCENARIOS AND CLIMATE MODELS

3.2.1 FUTURE SCENARIOS OF GREENHOUSE GAS CONCENTRATIONS

The future of anthropogenic greenhouse gas and aerosol emissions (and hence their resultant radiative forcing) is highly uncertain, encompassing substantial unknowns in population and economic growth, technological developments and transfer, and political and social changes. The climate modelling community has developed Representative Concentration Pathways (RCPs) to explore credible future options.

The four RCPs used in this Report represent the distillation of a much larger number of potential futures discussed in the literature (van Vuuren *et al*. 2011, Meinshausen *et al*. 2011). Each prescribes internally self-consistent 'representative' concentrations of greenhouse gases and aerosols, as well as land use changes. They were developed by a group of experts in areas spanning atmospheric modelling, chemistry and the carbon cycle and social scientists working in economics, policy and impacts (Moss *et al*. 2010). They are used in the fifth Climate Model Intercomparison Project (CMIP5) (refer Section 3.3) and the latest IPCC Assessment Report (2013).

The (estimated) carbon emissions and the corresponding radiative forcing for the four RCPs are shown in Figure 3.2.1.

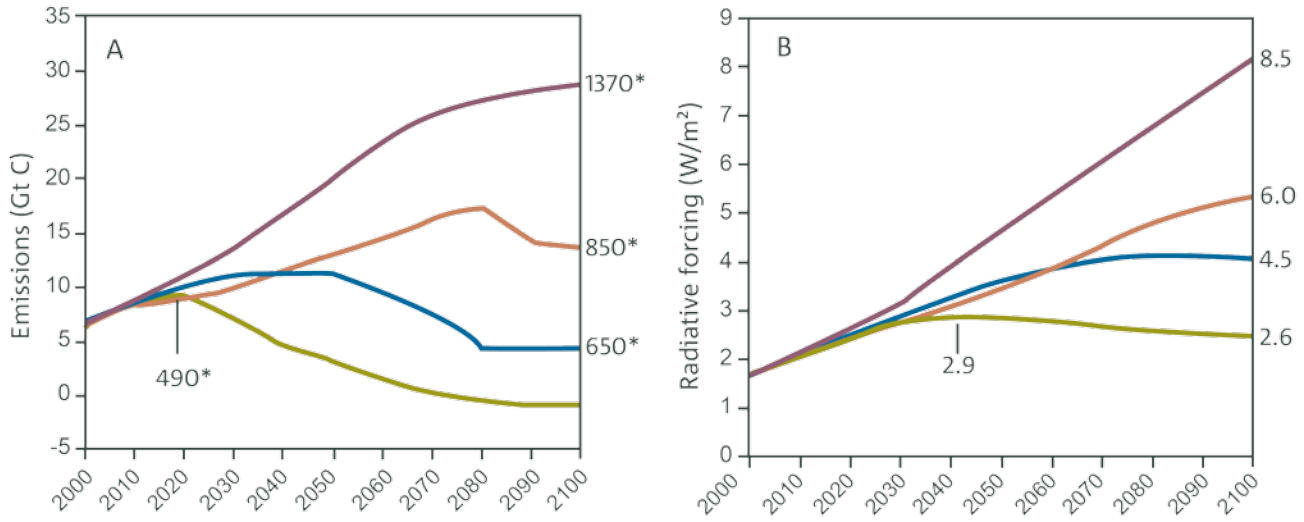

FIGURE 3.2.1: (A) EMISSIONS OF CARBON, IN GIGATONS FOR THE DIFFERENT RCP SCENARIOS USED IN THIS REPORT. THE ASTERISKED NUMBERS SHOW THE ATMOSPHERIC CO_2 EQUIVALENT[1] LEVELS IN PARTS PER MILLION (PPM). (B) RADIATIVE FORCING (SEE SECTION 3.1 FOR DEFINITION) FOR THE DIFFERENT SCENARIOS. THE NUMBERS ON THE RIGHT HAND AXIS SHOW THE FINAL FORCING (W/M^2) AND EQUATE TO THE NAMES OF THE RCP SCENARIOS. DRAWN FROM DATA AVAILABLE AT HTTP://WWW.PIK-POTSDAM.DE/~MMALTE/RCPS/.

RCPs differ from the Special Report on Emissions Scenarios (SRES) scenarios (Nakicenovic and Swart, 2000) used in the previous Climate Change in Australia (CSIRO and BOM, 2007) projections report and in the IPCC (2007) report). A comparison of carbon dioxide concentrations for the two sets of scenarios is shown in Figure 3.2.2. The RCPs represent a wider set of futures than SRES, and now explicitly include the effect of mitigation strategies. As with SRES, no particular scenario is deemed more likely than the others, however, some require major and rapid change to emissions to be achieved.

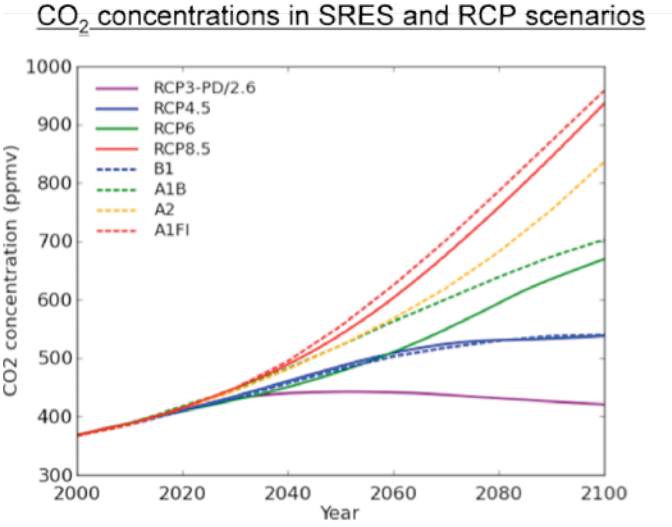

FIGURE 3.2.2: A COMPARISON OF RCPS AND SRES: CO_2 CONCENTRATIONS. NOTE THAT THESE ARE CO_2 ALONE, NOT THE "CO_2 EQUIVALENT" CONCENTRATIONS SHOWN ON THE RIGHT HAND AXIS OF FIGURE 3.2A. DRAWN FROM DATA AVAILABLE AT HTTP://WWW.PIK-POTSDAM.DE/~MMALTE/RCPS/.

1 CO_2 equivalent is the carbon dioxide concentration that would cause the same level of radiative forcing from all greenhouse gasses in the atmosphere (including methane, nitrous oxide and halocarbons).

RCP8.5 represents a future with little curbing of emissions, with a CO_2 concentration continuing to rapidly rise, reaching 940 ppm by 2100. Resultant forcing is close to that of SRES A1FI (Figure 3.2.2). RCP6.0 represents lower emissions, achieved by application of some mitigation strategies and technologies (van Vuuren *et al*. 2011). This scenario results in the CO_2 concentration rising less rapidly than RCP8.5, but still reaching 660 ppm by 2100 and total radiative forcing stabilising shortly after 2100. RCP4.5 concentrations are slightly above those of RCP6.0 until after mid-century, but emissions peak earlier (around 2040), and the CO_2 concentration reaches 540 ppm by 2100. Carbon dioxide concentrations under RCP4.5 closely mimic those of SRES scenario B1, the lowest emission scenario considered in the previous report (Figure 3.2.2). RCP2.6 (which can also be referred to as RCP3-PD for 'peak and decline') is the most ambitious mitigation scenario, with emissions peaking early in the century (around 2020), then rapidly declining. Such a pathway would require early participation from all emitters, including developing countries, as well as the application of technologies for actively removing carbon dioxide from the atmosphere (IGBP, 2010). The CO_2 concentration reaches 440 ppm by 2040 then slowly declines to 420 ppm by 2100). There was no equivalent scenario under SRES.

There are implications for projection uncertainties from the change in scenarios from the last report. RCPs begin with concentration levels, rather than with socio-economic assumptions followed by inferred emissions. As a result, uncertainties due to the response of the carbon cycle did not need to be factored into climate projections, as they do with the use of SRES scenarios. Consequently uncertainties due to the carbon cycle are not included in the projections in this Report. Instead, those uncertainties must now be factored into the mitigation strategies required to achieve particular concentration pathways (Rogelj *et al*. 2012). Such mitigation uncertainties lie outside the scope of this Report but are discussed and evaluated at length in IPCC (2014).

3.2.2 GLOBAL CLIMATE MODELS

Future climate changes cannot be simply extrapolated from past climate and further, and will depend on future concentration pathways. The best tools for climate change projections are general circulation models also called global climate models (GCMs). These are mathematical representations of the climate system run on powerful computers. Their fundamentals are based on the laws of physics, including conservation of mass, energy and momentum. GCMs are closely related to models used by the Bureau of Meteorology to produce Australia's weather forecasts.

GCMs represent the atmosphere and ocean as three-dimensional grids, with a typical atmospheric resolution of around 200 km, and 20 to 50 levels in the vertical. Models explicitly represent large-scale synoptic features of the atmosphere, such as the progression of high and low pressure systems, and large-scale oceanic currents and overturning. However many important physical processes occur at finer spatial scales. Examples include radiation and precipitation processes, cloud formation and atmospheric and oceanic turbulence. The impacts of such processes are included in 'parameterisations', whereby their effects are expressed in approximate form on the coarser model grid. Parameterisations are typically the result of intensive theoretical and observational study, and essentially represent an additional detailed physical modelling within the climate model itself.

Climate models have undergone continuous development for the last three decades, and now incorporate interactions between the atmosphere, oceans, sea ice and land surface. The schematics of a typical GCM are shown in Figure 3.2.3.

Some latest generation models can additionally represent the interactions between oceanic, atmospheric and land surface carbon cycles, including interactive atmospheric chemistry and vegetation (depicted in Figure 3.2.3). These models are evolving towards full 'Earth System Models'. For the RCP scenario experiments used in this Report however, all models were run with specified atmospheric trace gas concentrations.

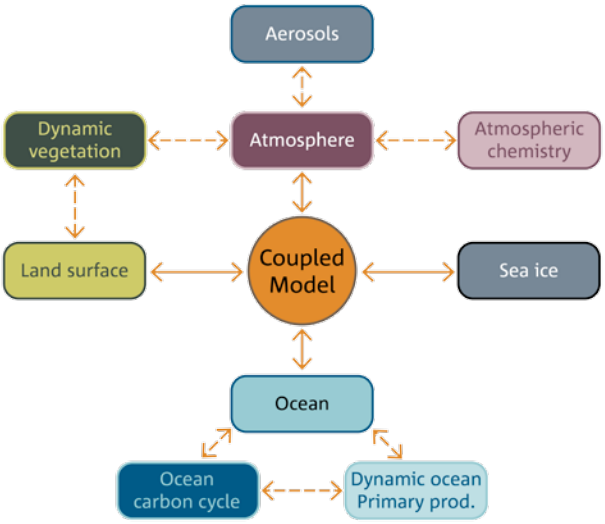

FIGURE 3.2.3: SCHEMATIC OF A GLOBAL COUPLED MODEL (GCM). CONTINUOUS LINES SHOW INTERACTIONS WITH COMPONENTS IN ALL COUPLED MODELS USED IN THIS REPORT. DASHED LINES SHOW INTERACTIONS INCLUDED IN SOME COUPLED MODELS.

Confidence in the use of models for projections comes from their basis in fundamental physical principles and from their ability to represent important features of the current and past climate (see Chapter 5). Over several generations of model development, GCMs have shown a substantial and robust warming due to increases in greenhouse gases. However, uncertainties in the details and timing of changes arise. These differences arise from uncertainties in how to represent some processes in models, and the resulting confidence in projections is greater for some variables

(*e.g.* temperature) than others (*e.g.* rainfall). These uncertainties are partly reflected in the ranges presented for projections in this Report. Also, while most models perform reasonably well, there is no single "best" model or subset of models, and climate projections differ between models.

Although model resolution has improved since the 2007 Australian projections, grid scales of global models limit representation of some important regional and local scale features of topography and coastline. These can be important for the local distribution of rainfall, for example. To better represent such features, techniques for downscaling can be applied, whereby finer resolution regional models are embedded within a global model, or where statistical relationships between local-scale climate and broad-scale climate features are exploited. Downscaling methods used in this Report, and their implications for projections, are discussed in Section 6.3.

3.3 INTRODUCTION TO CLIMATE MODEL ENSEMBLES AND TO THE CMIP5 ENSEMBLE

In order to support a systematic evaluation of climate models and their simulated future climate, a standardised set of model simulations (often also called experiments) is necessary. Since a large group of modelling centres around the world run this suite of simulations, the details of model performance can be assessed more readily. Some of the simulations are aimed at testing each model's ability to simulate the observed climate (called historical simulations) in order to assess confidence in climate model performance as a whole. Sets of additional simulations allow comparison of climate change under standard scenarios of future emission scenarios or concentrations pathways.

The international Model Intercomparison Projects (MIPs) have provided this experimental setup over the past two decades and the latest intercomparison is the Coupled Model Intercomparison Project Phase 5 (CMIP5; see http://cmip-pcmdi.llnl.gov/cmip5/ for more specific details). Simulations of future climate use the RCPs introduced in Section 3.2). The recently published Working Group One (WGI) report of the IPCC Fifth Assessment (IPCC, 2013) made extensive use of experiments from both CMIP5 and the previous intercomparison project (CMIP3) (Meehl *et al*. 2007).

There are several advantages in using a standard benchmark of experiments, including:

- The possibility to compare historical simulations with observations (exploring model skill)
- The possibility to compare model projections with each other (exploring the range of future climates)
- To isolate common strengths and weaknesses of each model
- To identify systematic errors (*e.g.* similar errors occurring in many models) from single model errors (to inform future model selection for impact assessment and model development and improvement)

The projections presented in this Report are based on analysis of the CMIP5 ensemble, and this ensemble is described in more detail in the next section.

3.3.1 THE COUPLED MODEL INTERCOMPARISON PROJECT PHASE 5 (CMIP5)

This section gives an overview of the current status of the CMIP5 model ensemble with respect to its overall properties and how it compares to CMIP3 – the previous generation of global climate models. There will be a more detailed examination of the capability of CMIP5 models to simulate the current climate, especially the Australian climate, in Chapter 5.

Table 3.3.1 provides a summary of the ocean-atmosphere general circulation models that were utilised in CMIP5 and CMIP3, including the horizontal grid resolution for the ocean and atmosphere components (in degrees) and the size of a single atmosphere grid cell (in km). There were simulations from 23 GCMs available from the CMIP3 experiments, which have now increased to 48 for the CMIP5 experiments. The archived data amount is extremely large and the analysis will take several years by the global science community since only a fraction of the overall data has been collected worldwide. However, a large group of models have already lodged data sets from the historical period and the future emission scenarios in the archive.

At the time of writing, CMIP5 was still active and model data were still being submitted to the CMIP5 archive. As such, the analysis contributing to this Report has been limited to the set of models in Table 3.3.1. Not all these models currently provide data for all variables of interest and thus it is necessary to use a smaller set of models in many individual analyses. In Table 3.3.2 the list of atmospheric monthly and daily variables from the different experiments used in this Report is shown for five experiments (one historical and four future experiments using the RCPs) along with the number of models used for the standard projection results for each of the variables.

TABLE 3.3.1: LIST OF CMIP5 AND CMIP3 OCEAN-ATMOSPHERE GENERAL CIRCULATION MODELS INCLUDING THE GRID RESOLUTION FOR THE OCEAN AND ATMOSPHERE COMPONENTS (IN DEGREES) AND THE SIZE OF A SINGLE ATMOSPHERE GRID CELL (IN KM). MODELS USED AS INPUT INTO DOWNSCALING STUDIES ARE MARKED (DOWNSCALING BY # BUREAU OF METEOROLOGY STATISTICAL DOWNSCALING MODEL, * CUBIC CONFORMAL ATMOSPHERIC MODEL (SEE SECTION 6.3)).

CMIP5 MODEL ID	INSTITUTE AND COUNTRY OF ORIGIN	OCEAN HORIZONTAL RESOLUTION (°LAT X °LON)	ATMOSPHERE HORIZONTAL RESOLUTION (°LAT X °LON)	ATMOSPHERE RESOLUTION (AT THE EQUATOR)	
				LATITUDE (KM)	LONGITUDE (KM)
ACCESS-1.0 # *	CSIRO-BOM, Australia	1.0×1.0	1.9×1.2	210	130
ACCESS-1.3 #	CSIRO-BOM, Australia	1.0×1.0	1.9×1.2	210	130
BCC-CSM1-1	BCC, CMA, China	1.0×1.0	2.8×2.8	310	310
BCC-CSM1-1-M #	BCC, CMA, China	1.0×1.0	1.1×1.1	120	120
BNU-ESM #	BNU, China	0.9×1.0	2.8×2.8	310	310
CanCM4	CCCMA, Canada	1.4×0.9	2.8×2.8	310	310
CanESM2 #	CCCMA, Canada	1.4×0.9	2.8×2.8	310	310
CCSM4 # *	NCAR, USA	1.1×0.6	1.2×0.9	130	100
CESM1-BGC	NSF-DOE-NCAR, USA	1.1×0.6	1.2×0.9	130	100
CESM1-CAM5	NSF-DOE-NCAR, USA	1.1×0.6	1.2×0.9	130	100
CESM1-FASTCHEM	NSF-DOE-NCAR, USA	1.1×0.6	1.2×0.9	130	100
CESM1-WACCM	NSF-DOE-NCAR, USA	1.1×0.6	2.5×1.9	275	210
CMCC-CESM	CMCC, Italy	2.0×1.9	3.7×3.7	410	410
CMCC-CM	CMCC, Italy	2.0×1.9	0.7×0.7	78	78
CMCC-CMS #	CMCC, Italy	2.0×2.0	1.9×1.9	210	210
CNRM-CM5 # *	CNRM-CERFACS, France	1.0×0.8	1.4×1.4	155	155
CNRM-CM5-2	CNRM-CERFACS, France	1.0×0.8	1.4×1.4	155	155
CSIRO-Mk3-6-0 #	CSIRO-QCCCE, Australia	1.9×0.9	1.9×1.9	210	210
EC-EARTH	EC-EARTH, Europe	1.0×0.8	1.1×1.1	120	120
FIO-ESM	FIO, SOA, China	1.1×0.6	2.8×2.8	310	310
GFDL-CM2p1	NOAA, GFDL, USA	1.0×1.0	2.5×2.0	275	220
GFDL-CM3 *	NOAA, GFDL, USA	1.0×1.0	2.5×2.0	275	220
GFDL-ESM2G #	NOAA, GFDL, USA	1.0×1.0	2.5×2.0	275	220
GFDL-ESM2M #	NOAA, GFDL, USA	1.0×1.0	2.5×2.0	275	220
GISS-E2-H	NASA/GISS, NY, USA	2.5×2.0	2.5×2.0	275	220
GISS-E2-H-CC	NASA/GISS, NY, USA	1.0×1.0	1.0×1.0	110	110
GISS-E2-R	NASA/GISS, NY, USA	2.5×2.0	2.5×2.0	275	220
GISS-E2-R-CC	NASA/GISS, NY, USA	1.0×1.0	1.0×1.0	110	110
HadCM3	MOHC, UK	1.2×1.2	3.7×2.5	410	280
HadGEM2-AO	NIMR-KMA, Korea	1.0×1.0	1.9×1.2	210	130
HadGEM2-CC #	MOHC, UK	1.0×1.0	1.9×1.2	210	130
HadGEM2-ES	MOHC, UK	1.0×1.0	1.9×1.2	210	130
INMCM4	INM, Russia	0.8×0.4	2.0×1.5	220	165
IPSL-CM5A-LR #	IPSL, France	2.0×1.9	3.7×1.9	410	210
IPSL-CM5A-MR #	IPSL, France	1.6×1.4	2.5×1.3	275	145
IPSL-CM5B-LR #	IPSL, France	2.0×1.9	3.7×1.9	410	210
MIROC4h	JAMSTEC, Japan	0.3×0.2	0.56×0.56	60	60

MIROC5 #	JAMSTEC, Japan	1.6×1.4	1.4×1.4	155	155
MIROC-ESM #	JAMSTEC, Japan	1.4×0.9	2.8×2.8	310	310
MIROC-ESM-CHEM #	JAMSTEC, Japan	1.4×0.9	2.8×2.8	310	310
MPI-ESM-LR #	MPI-N, Germany	1.5×1.5	1.9×1.9	210	210
MPI-ESM-MR #	MPI-N, Germany	0.4×0.4	1.9×1.9	210	210
MPI-ESM-P	MPI-N, Germany	1.5×1.5	1.9×1.9	210	210
MRI-CGCM3 #	MRI, Japan	1.0×0.5	1.1×1.1	120	120
MRI-ESM1	MRI, Japan	1.0×0.5	1.1×1.1	120	120
NorESM1-M # *	NCC, Norway	1.1×0.6	2.5×1.9	275	210
NorESM1-ME	NCC, Norway	1.1×0.6	2.5×1.9	275	210

CMIP3 MODEL ID	INSTITUTE AND COUNTRY OF ORIGIN	OCEAN HORIZONTAL RESOLUTION (°LAT X °LON)	ATMOSPHERE HORIZONTAL RESOLUTION (°LAT X °LON)	ATMOSPHERE RESOLUTION (AT THE EQUATOR)	
				LATITUDE (KM)	LONGITUDE (KM)
bccr-bcm2-0	BCCR, Norway	1.0×1.0	2.8×2.8	310	310
cccma-cgcm3-1	CCCMA, Canada	1.9×1.9	3.7×3.7	410	410
cccma-cgcm3-1-t63	CCCMA, Canada	1.4×0.9	2.8×2.8	310	310
cnrm-cm3	CNRM, France	2.0×1.0	2.8×2.8	310	310
csiro-mk3-0	CSIRO, Australia	1.9×0.9	1.9×1.9	210	210
csiro-mk3-5	CSIRO, Australia	1.9×0.9	1.9×1.9	210	210
gfdl-cm2-0	NOAA, GFDL, USA	1.0×1.0	2.5×2.0	275	220
gfdl-cm2-1	NOAA, GFDL, USA	1.0×1.0	2.5×2.0	275	220
giss-aom	NASA/GISS, USA	4.0×3.0	4.0×3.0	440	330
giss-model-e-h	NASA/GISS, USA	1.0×1.0	5.0×4.0	550	440
giss-model-e-r	NASA/GISS, USA	5.0×4.0	5.0×4.0	550	440
iap-fgoals1-0-g	IAP, China	1.0×1.0	2.8×2.8	310	310
ingv-echam4	INGV, Italy	1.0×1.0	1.1×1.1	120	120
inmcm3-0	INM, Russia	2.5×2.0	5.0×4.0	550	440
ipsl-cm4	IPSL, France	2.0×1.0	3.7×2.5	410	280
miroc3-2-hires	CCSR, Japan	1.2×0.6	1.1×1.1	120	120
miroc3-2-medres	CCSR, Japan	1.4×0.9	2.8×2.8	310	310
miub-echo-g	MIUB, Germany/Korea	2.8×2.3	3.7×3.7	410	410
mpi-echam5	MPI-M, Germany	1.0×1.0	1.9×1.9	210	210
mri-cgcm2-3-2a	MRI, Japan	2.5×2.0	2.8×2.8	310	310
ncar-ccsm3-0	NCAR, CO, USA	1.1×0.5	1.4×1.4	155	155
ncar-pcm1	NCAR, CO, USA	1.0×1.0	2.8×2.8	310	310
ukmo-hadcm3	MOHC, UK	1.2×1.2	3.8×2.5	420	280

TABLE 3.3.2: LIST OF AVAILABLE SIMULATIONS FROM CMIP5 OCEAN-ATMOSPHERE GENERAL CIRCULATION MODELS FOR NINE MONTHLY (TOP SECTION) AND EIGHT DAILY (EXTREMES; BOTTOM SECTION) CLIMATE VARIABLES FROM 5 DIFFERENT EXPERIMENTS. THE CLIMATE VARIABLES ARE: *HURS* = SURFACE RELATIVE HUMIDITY; *PR* = PRECIPITATION; *PSL* = SURFACE PRESSURE; *RSDS* = SURFACE DOWNWARD SOLAR RADIATION; *TAS* = SURFACE AIR TEMPERATURE; *TASMIN* AND *TASMAX* = MINIMUM AND MAXIMUM SURFACE AIR TEMPERATURE; *UAS* AND *VAS* = SURFACE ZONAL AND MERIDIONAL WINDS; *RX1DAY* = ANNUAL MAXIMUM 1-DAY RAINFALL; *RX1DAY-RV20* = 20 YEAR RETURN VALUE FOR RX1DAY; *TXX* = ANNUAL MAXIMUM DAILY MAXIMUM TEMPERATURE; *TXX-RV20* = 20 YEAR RETURN VALUE FOR TXX; *TNN* = ANNUAL MINIMUM DAILY MINIMUM TEMPERATURE; *TNN-RV20* = 20 YEAR RETURN VALUE FOR TNN; *SFCWINDMAX* = ANNUAL MAXIMUM SURFACE WIND SPEED; *SFCWINDMAX-RV20* = 20 YEAR RETURN VALUE OF SFCWINDMAX.

MONTHLY fields	hurs	pr	psl	rsds	tas	tasmax	tasmin	uas	vas
HISTORICAL	37	47	46	45	46	42	42	19	19
RCP4.5	31	38	38	37	38	36	36	23	23
RCP8.5	30	39	39	39	37	37	36	24	24
RCP6.0	18	21	21	21	21	20	19	13	13
RCP2.6	20	28	27	26	28	24	24	18	18

DAILY fields (extremes)	rx1day	rx1day-RV20	txx	txx-RV20	tnn	tnn-RV20	sfcWind max	sfcWind max-RV20	
HISTORICAL	25	25	27	27	27	27	22	22	
RCP4.5	21	22	23	24	23	23	18	15	
RCP8.5	24	24	25	26	26	26	18	17	
RCP6.0	-	-	-	-	-	-	3	3	
RCP2.6	-	-	-	-	-	-	12	12	

Not all modelling centres made the same data fields available and there are (at the time of writing) gaps in the data archive globally. For example, while there are monthly rainfall data from 48 models, the maximum 1-day rainfall is only available from 31 models, highlighting the fact that different modelling centres have different priorities with respect to which model output they can contribute.

The climate models that participated in the CMIP3 experiment have been widely described in the literature over the last five years (*e.g.* Randall *et al*. 2007). Some of the modelling institutes have since improved the resolution in their models from CMIP3 to CMIP5 (*e.g.* CNRM, GISS, INM and MRI, see Table 3.3.1 for details). Overall, the average resolution has significantly improved from CMIP3 to CMIP5 and is shown for the atmospheric grid cells in Figure 3.3.1. The median size of an atmospheric grid cell has decreased from (300 x 300 km) to (200 x 200 km) and there are now global models in CMIP5 with sub-100 km grid cell size, which is approaching values usually seen in regional climate models.

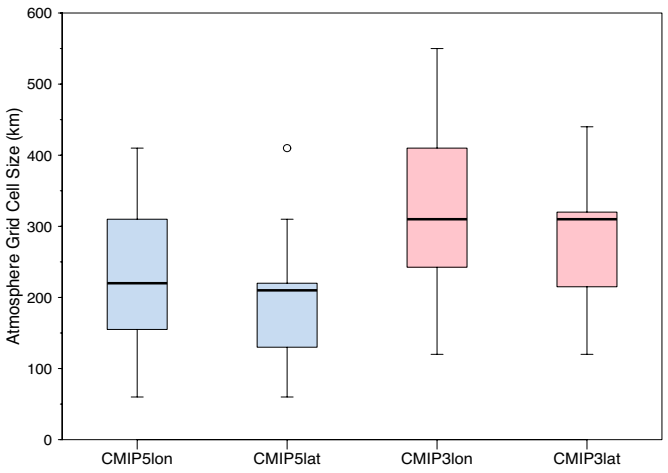

FIGURE 3.3.1: BOX-WHISKER PLOT OF GRID CELL SIZE (IN KM) IN GLOBAL CLIMATE MODEL'S ATMOSPHERE FOR CMIP5 MODELS (BLUE, FOR LONGITUDES AND LATITUDES; N=46) AND CMIP3 MODELS (PINK, N=23). THE BOX DISPLAYS THE MIDDLE 50 % OF THE MODELS WHILE THE WHISKERS SHOW THE RANGE. THE CENTRE LINE IS THE MEDIAN GRID CELL SIZE. THE CIRCLE REPRESENTS AN OUTLIER MODEL (*E.G.* A MODEL WITH MUCH LOWER RESOLUTION COMPARED TO THE OTHER MODELS).

From CMIP3 to CMIP5, a large number of additional experiments have been included and a more detailed description can be found in Taylor *et al*. (2012). Some of the new experiments now include a biogeochemical component accounting for carbon cycles in the land, atmosphere, and ocean (Earth System Models, see "ESM" in model names of Table 3.3.1).

Most of the CMIP3 and CMIP5 models have repeated historical (and future) experiments to form an ensemble with different initial conditions (the initial state is taken in different points of the pre-industrial simulation). This provides insight into the influence of natural variability on the simulations.

A subset of CMIP5 simulations are used to examine future greenhouse gas and aerosol scenarios called representative concentration pathways or RCPs in CMIP5 (see section 3.2). The size of this subset is given by the number of models that have simulated both the current and future climate for each forcing scenario (and for all variables of interest; see Table 3.3.2). For the majority of the projection results presented in this Report, RCP2.6, RCP4.5 and RCP8.5 are used as the contribution of model runs are more complete for these scenarios (Table 3.3.2).

There are far more models and more simulations in CMIP5 than there were in CMIP3. All model data have been accessed using the global Earth System Grid (ESG), which had been setup to facilitate the movement of large data amounts across many institutes (see https://www.earthsystemgrid.org/about/overview.htm for details about the ESG). The main archive in Australia – which is only a subset of all the CMIP5 data available across the ESG – is located in Canberra at the National Computing Infrastructure (NCI) facility (a collaboration between ANU, CSIRO, the Bureau of Meteorology and Geoscience Australia; see http://nci.org.au/ for details about the NCI facility) and has reached a size of over 284 terabytes – comprising over 730,000 climate data files. This is more than eight times the volume of data that was collected for CMIP3 analysis. Analysing such large data amounts requires specialised frameworks. The *Pipeline Framework* has been developed at the Centre for Australian Climate and Weather Research (CAWCR) and has been used for much of the CMIP5 processing and analysis for this Report (see https://trac.nci.org.au/trac/cawcr/wiki/pipeline/ for more information about the Pipeline Framework).

3.4 OBSERVED GLOBAL TRENDS AND THEIR ATTRIBUTION

The latest report of the IPCC WGI (2013) concluded that "warming of the climate system is unequivocal, and since the 1950s, many of the observed changes are unprecedented over decades to millennia. The atmosphere and ocean have warmed, the amounts of snow and ice have diminished, sea level has risen, and the concentrations of greenhouse gases have increased". Figure 3.4.1 (from IPCC, 2013) shows the observed global temperature record from 1850. Observed global mean temperature has risen by around 0.85 °C from 1880 to 2012, at a rate of around 0.12 °C per decade since 1951 (IPCC, 2013).

Increasing greenhouse gases have been the dominant cause of these observed changes to the climate system, along with smaller contributions from natural and other human influences.

Formal attribution has typically been based on research that uses a combination of climate modelling, instrumental climate observations, physical understanding and sometimes palaeoclimate reconstructions (use of proxies such as tree rings and ice cores to establish climate over Earth's history) to investigate cause and effect in a climate change context.

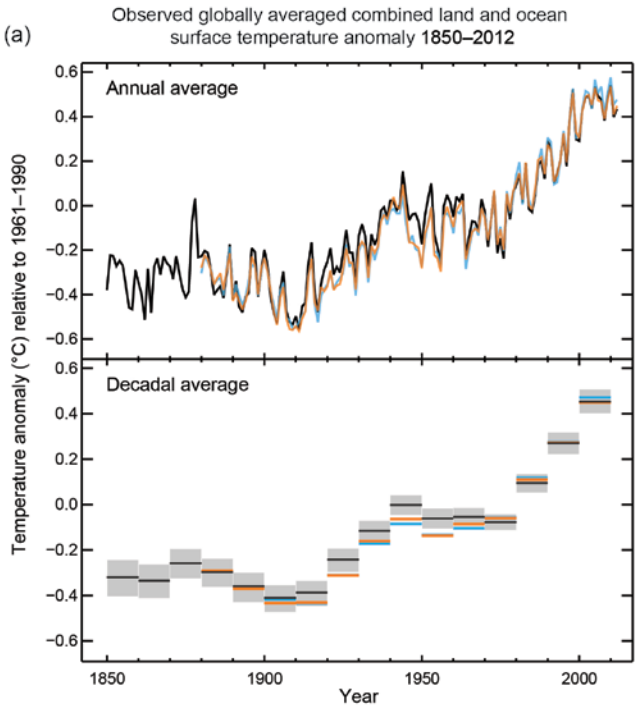

FIGURE 3.4.1: OBSERVED GLOBAL MEAN COMBINED LAND AND OCEAN SURFACE TEMPERATURE ANOMALIES (RELATIVE TO 1961-1990), FROM 1850 TO 2012 FROM THREE DATA SETS, WITH THE TOP PANEL GIVING ANNUAL MEAN VALUES AND THE LOWER PANEL DECADAL MEANS WITH AN UNCERTAINTY IN GREY FOR ONE DATA SET (SOURCE: FIGURE SPM.1A IN IPCC, 2013).

Specifically, climate models are used to characterise both natural internal climate variability as well as changes to the climate system that are driven by changes in one or more forcing mechanisms, such as changes in greenhouse gases, changes in solar radiation and changes in volcanic aerosols. This process determines climate change 'signals' (or 'responses') associated with changes in forcing parameters that are preferably unique to those parameters. A detailed comparison of observed changes with climate model derived signals, also known as climate change fingerprints, forms the basis of formal attribution studies.

Using a variety of methods, climate change attribution also seeks to clearly distinguish intrinsic modes of climate variability such as the El Niño-Southern Oscillation, from externally forced climate change and determine the dominant causes of the observed climate change over the last century or more.

For the Second and Third IPCC WGI Assessment Reports (IPCC, 1995, IPCC, 2001), robust attribution was mostly limited to global climate change metrics. The Second Assessment Report in 1995 concluded, "The balance of evidence suggests a discernible human influence on climate". For the Third Assessment report, optimal fingerprints of climate change (or four-dimensional spatio-temporal climate indicators) provided "new and stronger evidence that most of the warming observed in the last 50 years is attributable to human activities".

This evidence strengthened in the two subsequent IPCC Reports. The Fifth IPCC Assessment Report (IPCC, 2013) concluded that it is extremely likely that human influence has been the dominant cause of the observed warming since the mid-20th century.

Of the observed global mean temperature increase of around 0.85 °C from 1880 to 2012 increasing greenhouse gases were likely responsible for between 0.5 °C and 1.3 °C of warming since 1951, an amount likely offset by other anthropogenic influences (mostly aerosols) responsible for temperature forcing of between -0.6 °C and 0.1 °C (IPCC, 2013). Natural forcings and intrinsic climate variability were determined to have had little influence on recent warming trends.

The Fourth and Fifth IPCC Assessment Reports included additional regional attribution studies. In general, regional attribution is much more difficult than attribution of global changes, since the signal-to-noise ratio (or the magnitude of climate change signals in comparison to intrinsic variability) is much smaller at the regional scale, where the influence of intrinsic climate modes of variability can be very large (Stott *et al*. 2010).

Similarly, while attribution of regional warming can be reasonably expected to be consistent with attribution of global warming, this is not the case for all climate variables. In the Australian context in particular, attributing rainfall changes is a difficult task due to the strong influence of natural drivers such as the El Niño-Southern Oscillation, and the inherently large range of Australian rainfall variability.

While these considerations continue to hamper efforts to firmly attribute observed regional changes, more recent studies have demonstrated that regional attribution is increasingly possible, as the signal of warming grows larger over time (Stott *et al*. 2010). Several studies have shown a substantial anthropogenic contribution to warming over every continent except Antarctica (Hegerl *et al*. 2007, Morice *et al*. 2012, Jones *et al*. 2013). The IPCC *Fifth Assessment Report* (IPCC, 2013) noted that further evidence has accumulated for the attribution of regional climate change. Large observational uncertainties continue to impact on the ability to firmly attribute the warming observed in Antarctica.

In addition to surface and tropospheric warming, the *Fifth Assessment Report* concludes that a human influence has also been detected on a number of other climate variables. It is very likely that human influences have made a substantial contribution to upper-ocean warming (above 700 m) and global mean sea level rise since the 1970s. Anthropogenic forcing is also very likely to have influenced Arctic sea-ice loss, reduction in ice sheets and glaciers, and reduction in Northern Hemisphere snow cover. A human influence is also increasingly detected on the global water cycle since 1960 (IPCC, 2013). In a warming climate, the atmosphere can hold more water vapour, around 7 % more for every degree of global warming. Such a change represents an intensification of the hydrological cycle, expressed as increased heavy rainfall and potential evaporation in climate models. There is emerging evidence, in regions with good quality observational data, that global warming has contributed to a global-scale intensification of heavy precipitation over the second half of the 20th century (Donat *et al*. 2013b).

The *Fifth Assessment Report* also finds strengthening evidence for human influence on temperature extremes since the IPCC's *Fourth Assessment Report* and *Special Report on Managing the Risks of Extreme Events and Disasters to Advance Climate Change Adaptation* (SREX) (IPCC, 2012). A recent analysis of northern hemisphere heatwaves has shown that very hot summers have increased in frequency approximately 10 fold since the 1950s (Hansen *et al*. 2012), and that a number of recent summer heatwaves (such as the European 2003 and Moscow 2010 heatwaves) have been so extreme that their probability of occurrence without global warming would be close to zero (Otto *et al*. 2012, Rahmstorf and Coumou, 2011, Stott *et al*. 2004).

3.5 GLOBAL CLIMATE CHANGE PROJECTIONS

In this section we describe global scale projections of climate change based largely on the recently released IPCC WGI *Fifth Assessment Report* (see Chapter 11, 12 and 14 in IPCC, 2013; also SPM in IPCC, 2013). The ENSO projections described below are updated in light of more recent literature (Power *et al*. 2013, Santoso *et al*. 2013)

The global average surface air temperature over the period 1850-2100 from the CMIP5 models is depicted in Figure 3.5.1. The values presented are anomalies relative to the average over the period 1986–2005. IPCC (2013) concluded that global mean surface air temperatures for 2081–2100 relative to 1986–2005 are likely to be in the following ranges: 0.3 to 1.7 °C for RCP2.6, 1.1 to 2.6 °C for RCP4.5, 1.4 to 3.1 °C for RCP6.0, and 2.6 to 4.8 °C for RCP8.5.

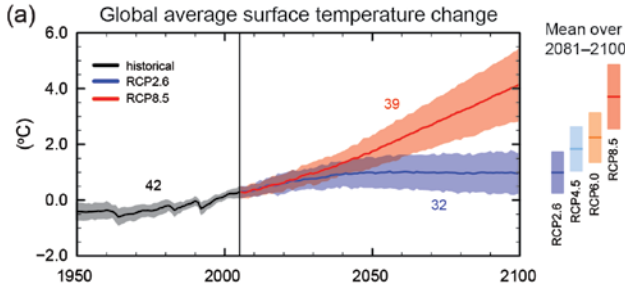

FIGURE 3.5.1: CHANGE IN GLOBAL ANNUAL MEAN SURFACE TEMPERATURE RELATIVE TO 1986-2005 AS SIMULATED BY CMIP5 MODELS. SHOWN IS THE TIME SERIES OF PROJECTIONS (BOLD LINES) AND UNCERTAINTY (SHADING) FOR SCENARIOS RCP2.6 (BLUE) AND RCP8.5 (RED). BLACK (GREY SHADING) IS THE MODELLED HISTORICAL EVOLUTION OF TEMPERATURE USING HISTORICAL RECONSTRUCTED FORCINGS. ON THE RIGHT HAND SIDE THE MEAN AND ASSOCIATED UNCERTAINTIES AVERAGED OVER 2081–2100 ARE GIVEN FOR ALL RCP SCENARIOS AS COLOURED VERTICAL BARS. THE NUMBERS OF CMIP5 MODELS USED TO CALCULATE THE MULTI-MODEL MEAN IS INDICATED (SOURCE: FIGURE SPM.7A IN IPCC, 2013).

It is important to realise that temperature changes could be higher than those depicted in Figure 3.5.1. For example, greenhouse gas concentrations might end up being larger than those assumed under the RCP8.5 scenario. Higher values might arise through the release of carbon dioxide or methane to the atmosphere from, for example, thawing permafrost from Arctic and sub-Arctic peat bogs over the 21st century. Some thawing has already occurred over Alaska, Canada and northern Russia and further thawing is expected. However, the magnitude of the increase in emissions from thawing over the 21st century is very uncertain. The latest IPCC report gave a range of 50 to 250 GtC (gigatons of carbon) over this century under the RCP8.5 scenario, but stated that confidence in this range is low. The global oceans will continue to remove anthropogenic CO_2 from the atmosphere independent of the future concentration pathway, which will lead to rising acidification of the oceans. The oceans will also continue to remove heat from the atmosphere in deeper ocean layers – a long-term process that will continue to warm the oceans for centuries (IPCC, 2013, Chapter 6).

REGIONAL CONTRASTS IN WARMING AND PRECIPITATION CHANGE

Global warming is not spatially uniform. This is illustrated in Figure 3.5.2, which shows the projected warming over the globe in 2081–2100 relative to 1986–2005 under the RCP2.6 and RCP8.5 scenarios. Under both scenarios warming tends to be greater over land than over the ocean, and warming tends to be greater over the Arctic than elsewhere. Warming tends to be weaker over several oceanic regions.

Precipitation patterns are projected to change. This is illustrated in Figure 3.5.2 (b) which shows the projected precipitation change over the globe in 2081–2100 relative to 1986–2005 under the RCP2.6 and RCP8.5 scenarios. Under both scenarios precipitation tends to increase at high latitudes and near the equator, with reductions projected to the south-west of Australia, South America and Africa, and over a band reaching from the Mid-Atlantic into the Mediterranean region.

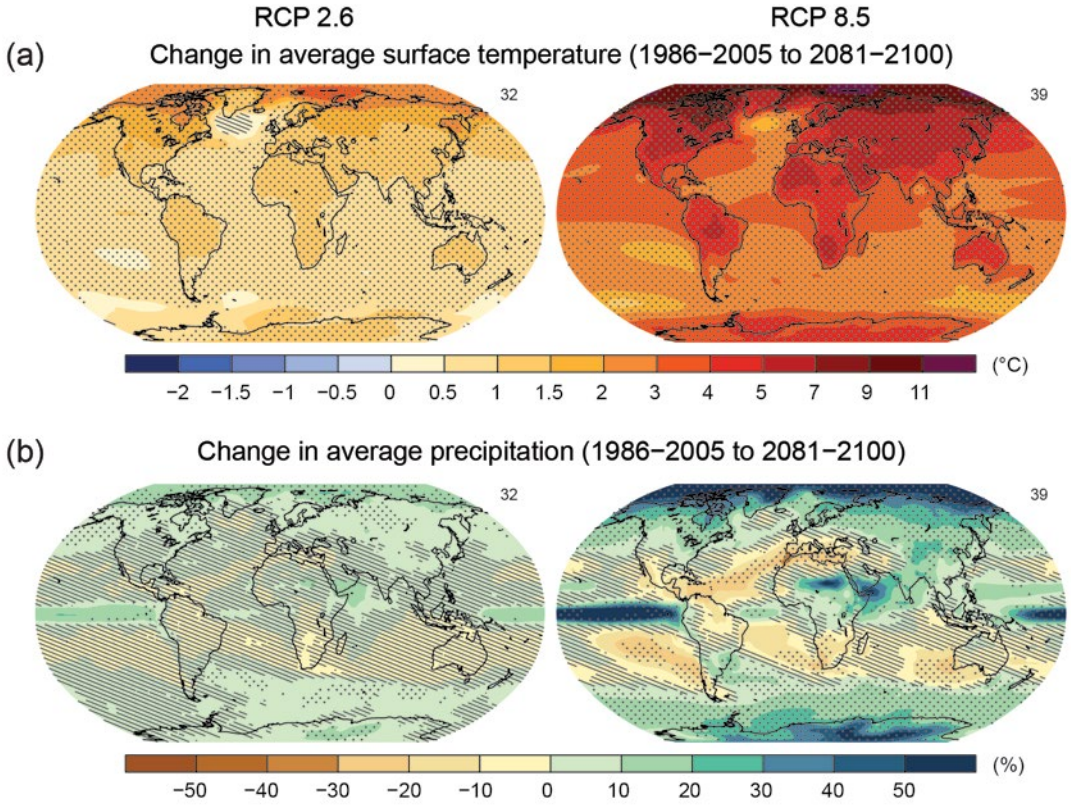

FIGURE 3.5.2: MAPS OF CMIP5 MULTI-MODEL MEAN RESULTS FOR THE SCENARIOS RCP2.6 AND RCP8.5 IN 2081-2100 OF (A) ANNUAL MEAN SURFACE TEMPERATURE CHANGE AND (B) AVERAGE PER CENT CHANGE IN ANNUAL MEAN PRECIPITATION. CHANGES ARE SHOWN RELATIVE TO 1986-2005. THE NUMBER OF CMIP5 MODELS USED TO CALCULATE THE MULTI-MODEL MEAN IS INDICATED IN THE UPPER RIGHT CORNER OF EACH PANEL. HATCHING INDICATES REGIONS WHERE THE MULTI-MODEL MEAN IS SMALL COMPARED TO INTERNAL VARIABILITY (*I.E.* LESS THAN ONE STANDARD DEVIATION OF INTERNAL VARIABILITY IN 20-YEAR MEANS). STIPPLING INDICATES REGIONS WHERE THE MULTI-MODEL MEAN IS LARGE COMPARED TO INTERNAL VARIABILITY (*I.E.* GREATER THAN TWO STANDARD DEVIATIONS OF INTERNAL VARIABILITY IN 20-YEAR MEANS) AND WHERE 90 % OF MODELS AGREE ON THE SIGN OF CHANGE (SOURCE: FIGURE SPM.8 IN IPCC, 2013).

Projected changes in temperature and precipitation for the next few decades show spatial patterns of change similar to those projected for the late 21st century described above, but with smaller magnitude. Internal variability will continue to be a major influence on climate, particularly in the near-term and at the regional scale.

PROJECTED CHANGES IN SELECTED CLIMATE FEATURES

The IPCC (2013) states that global warming will cause more hot and fewer cold days and seasons over most land areas (*virtually certain* in their assessment) and that heat waves will occur with a higher frequency and duration (*very likely* in their assessment). Occasional cold winter extremes will continue to occur. Additionally, extreme precipitation events over most of the mid-latitude land masses and over wet tropical regions will become more intense and more frequent by the end of this century, as global mean surface temperature increases (*very likely* assessment in IPCC, 2013). This increase stems mostly from the greater moisture holding capacity of a warmer atmosphere (IPCC, 2013) as well as a potential for increased vertical velocity of air masses under enhanced greenhouse warming (O'Gorman and Schneider, 2009).

The global monsoon system contributes greatly to the water cycle on Earth. The relevant regional monsoon system for Australia is described in more detail in Section 4.1, with projections in Chapter 7. On the global scale, however, the region affected by the monsoons is projected to increase over the 21st century, together with monsoon rainfall and intensity (IPCC, 2013, Chapter 12). These increases are understood to be related to the increases in atmospheric moisture under enhanced warming. At the same time, monsoon winds are projected to weaken due to the slowing of the global tropical circulation (IPCC, 2013, Chapter 12). Monsoon onset dates are projected to become earlier or not to change much, while monsoon retreat dates are projected to be delayed, resulting in lengthening of the monsoon season in many regions (IPCC, 2013, Chapter 12).

The IPCC report (Chapter 12 in IPCC, 2013) also concluded that "there is *high confidence* that the El Niño-Southern Oscillation (ENSO, see Section 4.1 for a more detailed

description) will remain the dominant mode of year to year variability in the tropical Pacific, with global effects in the 21st century. Due to the increase in moisture availability, ENSO-related precipitation variability on regional scales will *likely* intensify. Natural variations of the amplitude and spatial pattern of ENSO are large and thus *confidence* in any specific projected change in ENSO and related regional phenomena for the 21st century remains *low*". Additionally, more recent work concluded that global warming will intensify El Niño-driven drying in the western equatorial Pacific and further increase El Niño driven rainfall increases in the central and eastern Pacific during El Niño (Power *et al*. 2013, Cai *et al*. 2014).

The Indian Ocean Dipole (IOD, see Section 4.1 for a more detailed description) is associated with droughts in Indonesia, reduced rainfall over parts of Australia, intensified Indian summer monsoon, floods in East Africa, hot summers over Japan, and anomalous climate in the extra-tropical Southern Hemisphere (IPCC, 2013). Positive IOD has led to below average winter and spring rainfall across central and southern Australia. The overall frequency of IOD events (positive and negative) is not projected to change (Ihara *et al*. 2008, IPCC, 2013, Cai *et al*. 2013).

Changes in the Southern Annular Mode (SAM, see Section 4.1 for more detail) have an influence on the climate of Antarctica, Australasia, southern South America and South Africa (Watterson, 2009, Thompson *et al*. 2011 and references therein). In the past few decades the SAM index (describing the phase of this mode) has exhibited a positive trend in southern summer and autumn (Marshall, 2007, Jones *et al*. 2009b), a change attributed to the effects of ozone depletion and the increase in greenhouse gases (Thompson *et al*. 2011, IPCC, 2013). These two factors will continue to be the principal drivers into the future (assessed as likely in Chapter 14 in IPCC, 2013).

3.6 COMPARISON OF CMIP3 AND CMIP5 GLOBAL PROJECTIONS

The IPCC (2013, Chapter 12) provides a general comparison of CMIP3 and CMIP5 projections, but it is particularly worthwhile to compare the projections for Australia using the method applied in used in CSIRO and BOM (2007). As described further in Section 6.2 (and in Watterson, 2008), the comparison assumes that 'pattern scaling' applies, *i.e.* that there is a dominant climate change response pattern, and each location has a sensitivity or change 'per degree of global warming'. Consistent with this, it is assumed that a 'probability density function' (PDF) for change in a variable at a certain time and location can be obtained by combining a distribution for the global warming for that time with a distribution for the local sensitivity to warming. Maps of changes over Australia calculated using CMIP5 results are presented in later sections, and a comparison with maps from CMIP3 is made in Appendix A. The focus of this section is the difference between CMIP3 and CMIP5 on the larger scale, including the global warming.

3.6.1 GLOBAL SENSITIVITY OF THE CMIP3 AND CMIP5 MODELS

The probability distribution for the global warming used in the pattern scaling method provides a convenient representation of the global warming from the models. Given that the range of global surface warming from a model ensemble tends to be proportional to the median warming at the time (see for example CMIP5 results in Figure 3.5.1) it is assumed that a single shape of distribution holds for that ensemble. The shape has been derived from the near-linear trends during the 21st century projected under RCP8.5. The 100-year trend results from 40 CMIP5 models are shown in Figure 3.6.1. Three distributions for the change, which have the same mean and standard deviation as the ensemble, are shown. The beta form (a standard theoretical distribution), which also matches the range, is used as the global warming PDF. This CMIP5 PDF has a similar relative spread to the CMIP3 PDF (illustrated in CSIRO and BOM, 2007, Figure 4.6), with the ratio of the standard deviation to the mean being 19 % for CMIP5, compared to 21 % for CMIP3.

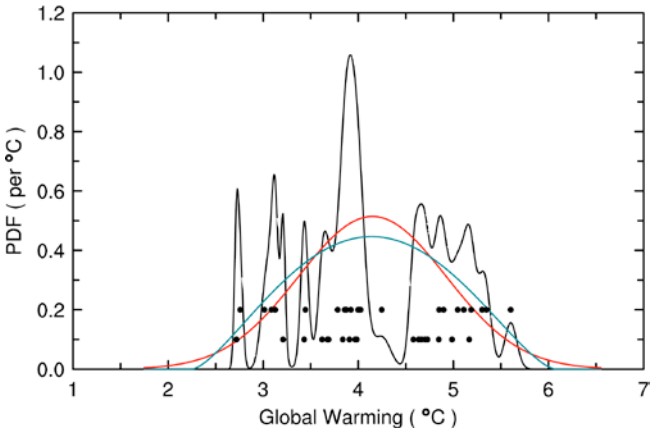

FIGURE 3.6.1: GLOBAL MEAN WARMING TRENDS (X 100 YEARS) OVER 2001–2100 FOR 40 CMIP5 MODELS, UNDER RCP8.5, SHOWN AS DOTS, WITH EARTH SYSTEM MODELS BEING THE UPPER SET. THE AVERAGE OF THE INDIVIDUAL PDFS (CENTRED ON EACH TREND, ALLOWING FOR STATISTICAL UNCERTAINTY) IS THE BLACK LINE. THE NORMAL DISTRIBUTION WITH THE SAME MEAN AND STANDARD DEVIATION IS RED. THE BETA FIT USED AS THE GLOBAL WARMING PDF IS BLUE.

The climate change from 1986–2005 to 2080–2099 under the RCP8.5 scenario is used as a standard case for presentation. The global warming from the multi-model mean is 3.7 °C, and the beta PDF has been scaled to have this mean. The 5th to 95th percentile range of the PDF is then 2.6 to 4.8 °C, which matches the range for this case given by the IPCC *Fifth Assessment Report* (IPCC, 2013).

The actual warming projected by a model depends on the forcing and the global sensitivity to it. Direct comparison of the CMIP3 and CMIP5 sensitivities is hampered by the different scenarios used (section 3.5). However, based on a range of studies and methods, the *Fifth Assessment Report* found that there is 'no fundamental difference' in the

overall sensitivities of the two ensembles. For the purpose of comparison in Appendix A, the beta PDF used in 2007 has been scaled to the same mean value of 3.7 °C.

The accuracy of the CMIP5 ensemble as representing the possible response of the real world has been assessed at length by the IPCC in the *Fifth Assessment Report* (IPCC, 2013), with particular consideration of the implications of the slower rate of warming in the past decade in estimates of the (real-world) global mean surface temperature. This is an active area of research with some recent work highlighting natural variability as likely to be the major cause of the difference between CMIP5 models' surface temperature and that observed in the past decade. England *et al*. (2014) found that an observed variation in winds over the Pacific Ocean, not captured by models, has led to enhanced uptake of heat by the subsurface ocean. They noted that if the winds returned to their usual state, there could potentially be a rapid upturn in surface temperature trends, similar to that which occurred after 1975.

However, given uncertainties in future ocean heat uptake, carbon cycle feedbacks and other processes not well represented in models (section 3.2.1), the *Fifth Assessment Report* authors assessed the existing CMIP5 range of global warming for 2080–2099 as a 'likely' range (more than 66 % probability), rather than the 90 % range from the PDF used here. A similar position was taken by the *Fourth Assessment Report*, in relation to the CMIP3 range, as used in the 2007 projections (IPCC, 2007).

3.6.2 MODEL RESPONSES TO GLOBAL WARMING IN THE ASIA–PACIFIC REGION

The local sensitivity to global warming used in the pattern scaling method is determined from the individual responses or 'change per degree' fields from models (see definition above). These are determined from yearly values over the whole 21st century. The fields from the CMIP3 and CMIP5 ensembles are compared here for the Asia-Pacific region that is especially important to Australian climate.

The ensemble mean and standard deviations for the temperature response (a non-dimensional ratio of local to global warmings) from CMIP3 and CMIP5 are shown in Figure 3.6.2. The patterns for both statistics are very similar. Over all land except for some coasts, the mean warming is larger than the global mean (as indicated by a value over one). The equatorial Pacific Ocean has relatively high values, but they are a little lower in CMIP5. High values also hold in the western Tasman Sea for both ensembles, while the Southern Ocean warms less. For both ensembles, the standard deviation over Australia and the central Pacific is double that of the regional ocean, except farther south. In fact, the variation in the 'NINO3.4' region (5°S-5°N, 170°W-120°W) is even larger in CMIP5. However, the result for CMIP5 is strongly affected by a single model (FGOALS-g2) that displays an unusual projection in this region.

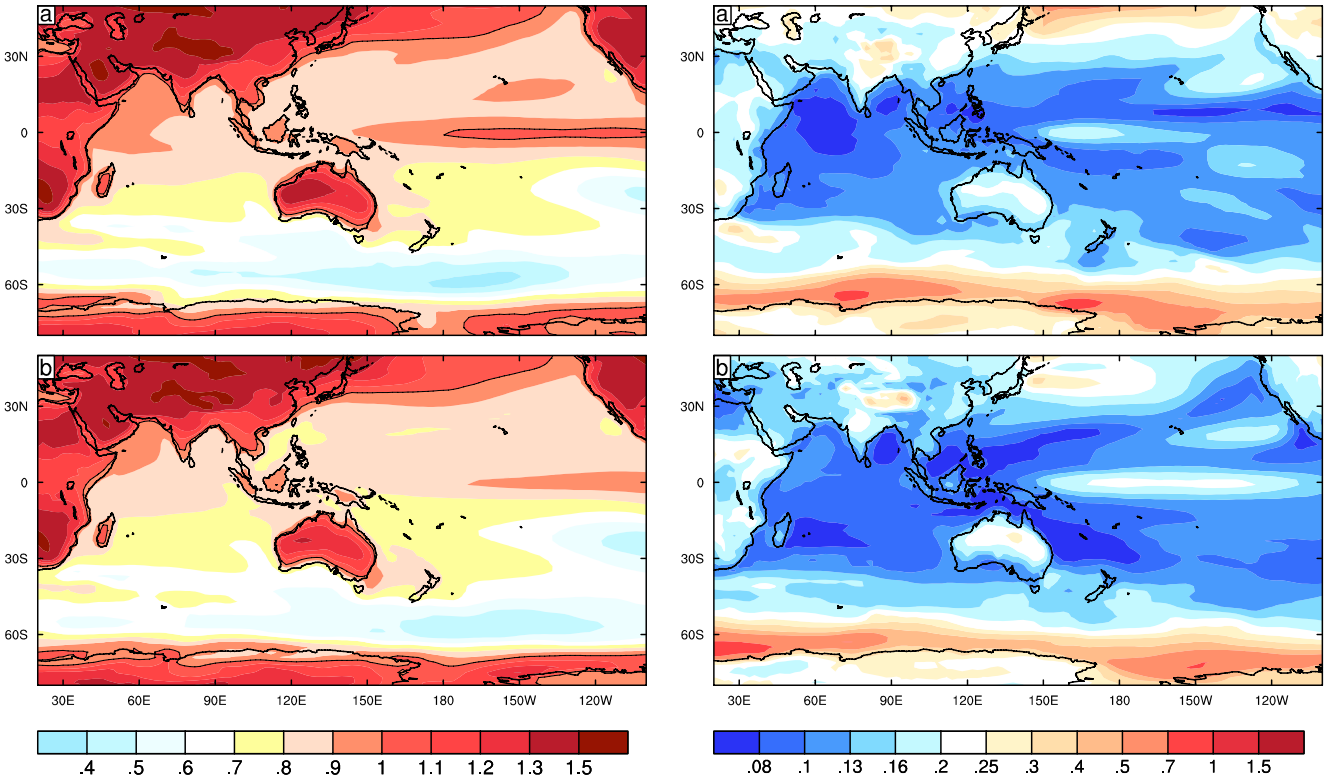

FIGURE 3.6.2: LEFT: ENSEMBLE MEANS OF THE TEMPERATURE 'CHANGE PER DEGREE' FIELDS (NON-DIMENSIONAL): (A) CMIP3 (24 MODELS) AND (B) CMIP5 (40 MODELS). RIGHT: THE ENSEMBLE STANDARD DEVIATIONS (A) CMIP3 AND (B) CMIP5.

Change per degree fields for rainfall, determined as a percentage of the present climate means of each model, have been evaluated, and again are similar in the two ensembles, as seen in Figure 3.6.3. Declines in the ensemble means occur in most of the sub-tropics, especially in the south-west of Australia. The decline in central and eastern Australia is smaller in CMIP5. Over most subtropical regions the standard deviation across each ensemble is relatively large, and changes of both signs occur in individual models.

These local sensitivities in temperature, rainfall and other variables, explain much of the spatial variation in the future changes. Furthermore, as shown by Watterson (2012) for CMIP3, much of the range of change over Australia can be linked to the range in the low-latitude ocean temperature changes, through ENSO and IOD-like patterns. With the ensemble mean warming in the NINO3.4 region being larger than in surrounding oceans (Figure 3.6.2b), the pattern in the mean change has often been described as 'El Niño-like'. Given the usual pattern of interannual variability in ENSO, the small mean drying over eastern Australia in the ensemble means (Figure 3.6.3b) could be interpreted as being a consequence of the El Niño-like change (see Section 4.1 for more detail on how these global modes of variability affect Australian climate). The range of the warming in the NINO3.4 region across the CMIP5 models, as inferred from Fig.3.6.2d, can likewise be inferred as driving part of the range in Australian future changes in rainfall and other variables.

The effect of this tropical sea surface temperature (SST) driver can be demonstrated by forming an index by area-averaging the individual annual change per degree fields (determined from the RCP8.5 simulations) over the NINO3.4 region. The correlation coefficient between the index values from 40 models with the Australian mean of the rainfall changes (in % per degree) from the models is −0.79. Correlations between the index and rainfall changes at most locations in eastern Australia are nearly as large. Thus models with a higher than average change in the index simulate a larger than average decline in rainfall. For CMIP3, Watterson (2012) found that an alternative tropical ocean index that quantified the difference between the western Pacific and east Indian Ocean temperature trends was even more effective. SST anomalies in these two regions tend to drive opposite directions of change in Australian rainfall. Even for CMIP5, this 'Pacific Indian Dipole' index has a correlation with Australian rainfall trends of −0.78. The variation in the east Indian region is smaller in CMIP5 (comparing Figures 3.6.2 a and b), but the dipole index still provides a simple description of the tropical SST driver: models that warm more/less in the Pacific than the Indian tend to have declining/increasing Australian rainfall. Ideally, assessments of mechanisms (such as that of Weller and Cai, 2013b) might provide insight into the possible realism of trends in such mode indices, and hence rainfall.

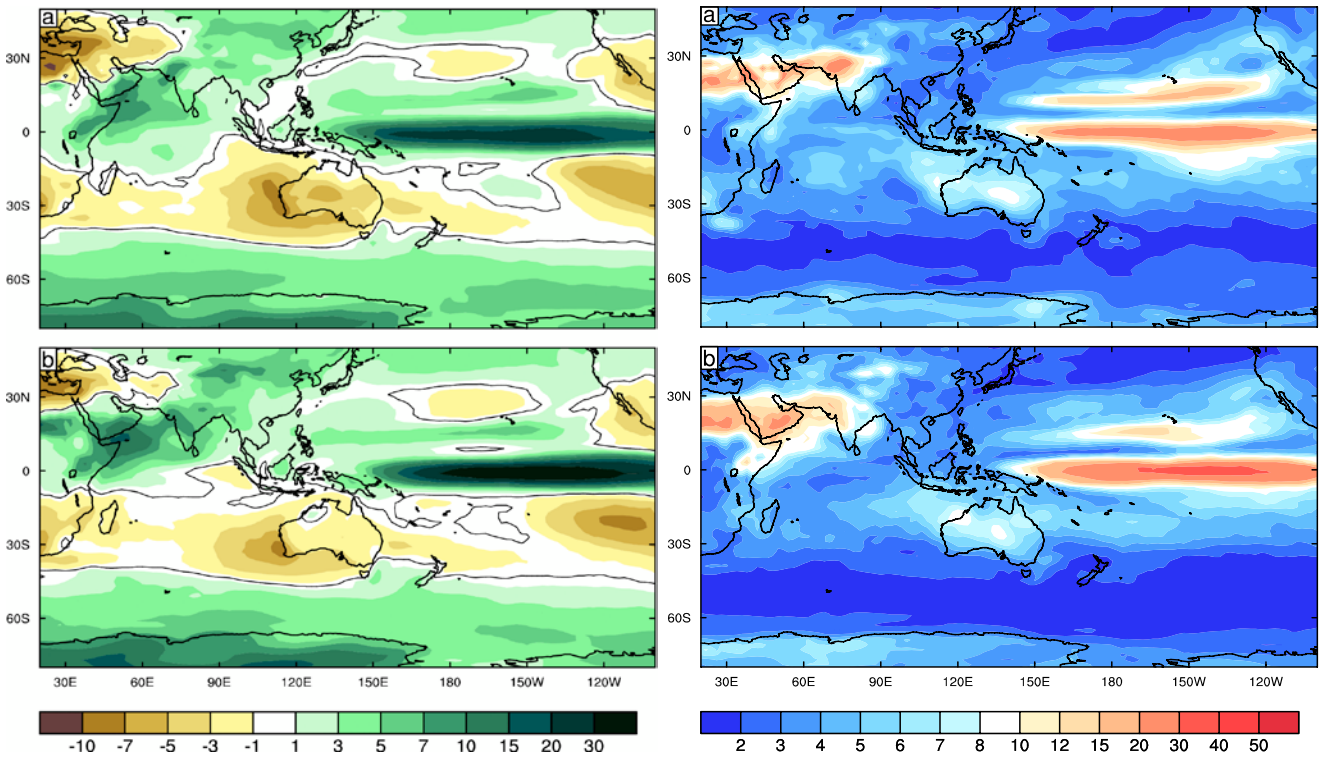

FIGURE 3.6.3: LEFT: ENSEMBLE MEANS OF THE RAINFALL 'CHANGE PER DEGREE (OF GLOBAL WARMING)' FIELDS (AS A PERCENTAGE OF PRESENT CLIMATE): (A) CMIP3 (24 MODELS) AND (B) CMIP5 (40 MODELS). RIGHT: THE ENSEMBLE STANDARD DEVIATIONS (A) CMIP3 AND (B) CMIP5.